© Indian Academy of Sciences

CrossMark

Optimal control of vibrational transitions of HCl

KRISHNA REDDY NANDIPATI* and ARUN KUMAR KANAKATI

School of Chemistry, University of Hyderabad, Hyderabad 500 046, India
*Corresponding author. E-mail: nkrishna88@gmail.com

Abstract. Control of fundamental and overtone transitions of a vibration are studied for the diatomic molecule, HCl. Specifically, the results of the effect of variation of the penalty factor on the physical attributes of the system (i.e., probabilities) and pulse (i.e., amplitudes) considering three different pulse durations for each value of the penalty factor are shown and discussed. We have employed the optimal control theory to obtain infrared pulses for selective vibrational transitions. The optimization of initial guess field with Gaussian envelope, phrased as maximization of cost functional, is done using the conjugate gradient method. The interaction of the field with the molecule is treated within the semiclassical dipole approximation. The potential and the dipole moment functions used in the calculations of control dynamics are obtained from high level *ab-initio* calculations.

1. Introduction

Many phenomena in chemistry, such as bond breaking and making, occur in ultrafast time-scale. The control of energy flow in a relatively short time-scale (~ 10 fs), in a nuclear degree of freedom that causes a particular relevant mode which involves bond breakage is a challenging task. Control of quantum phenomena using lasers has been a long-standing dream since their invention way back in 1960 [1]. Lasers have the advantage of depositing energy in a non-statistical fashion. Shaped femtosecond laser pulses, due to technological advancement of lasers, can be employed as a new class of reagents to alter the course of chemical reactions. The application of shaped pulses to control quantum processes has been successfully shown in experiments [2–4].

Theoretically, the design of optimal pulses can be formulated by utilizing the coherence property of laser light to steer the dynamics of a quantum system [5]. The two broad approaches to design such optimal pulses are the following. One approach in the time domain, was by Tannor and Rice [6,7] and the other in the frequency domain, by Brumer and Shapiro [8–10]. In the former approach, the frequencies, amplitudes and phases of the pulse (train of pulses) are tailored to steer the wave packet dynamically to reach the target state. This scheme has been experimentally demonstrated by Baumert and Gerber [11]. The latter approach is based on the principle of quantum mechanical interference between coherent optical excitation of multiple independent pathways and is demonstrated experimentally by Gordon and coworkers [12]. A variant of the Tannor–Rice scheme exploits control of amplitude, phase and interference (which is local in time) by pump–dump pulse seperation for the manipulation of population dynamics [13]. This leads to the interfering pathways interpretation of pump–dump scheme. Hence, pump–dump control can be viewed entirely from the perspective of Brumer–Shapiro formulation.

The most general mathematical framework for controlling the dynamics of a quantum system by designing suitable laser fields is formulated as quantum optimal control theory (QOCT) [14–16]. The control schemes mentioned earlier are special cases of this general theory. Within QOCT, both strong and weak field limits can be handled. QOCT seeks the best solution to a given problem under the stated goals with time-dependent Schrödinger equation as quantum system constraint along with other constraints. The problem of designing a pulse is phrased in terms of optimization of 'cost functional' which includes an objective term defining the dynamical goal, a penalty term that

accounts for minimization of laser fluence and a constraint to satisfy the dynamical equation of the system interacting with the field.

Many H-abstraction reactions in chemistry involve halides like HCl, HBr and HI. And they often need to undergo coherent vibrational excitation to promote the reaction (for instance, the late-barrier reactions in chemistry require vibrationally hot reactant molecules to have the reaction promoted) efficiently. This is the general motivation to study HCl. The second point, worth mentioning here, is that obtaining the correct dipole moment function, *ab-initio*, at large distances is difficult as one goes to higher halides. In this regard, here we were able to calculate the same for the HCl molecule and hence have made use of it to study vibrational transitions. This makes the calculations more rigourous and hence more useful in shaping infrared pulses. We hope that this serves well as a prototype for higher halides which participate in the kind of reactions mentioned above.

Extensive exploration of numerical approaches in developing iterative methods to solve quantum control equations in the area of QOCT has been done by Zhu *et al* [17]. Balint-kurti *et al* [18–20] used the conjugate gradient (CG) method [21] for optimization in the control of vibrational excitation of H_2 molecule where polarization forces are taken into account. Recently, studies of controlling HF fundamental and overtone excitations using an iterative method, the CG, and a genetic algorithm (GA) [22–24] have been applied by Singh *et al* [25] and the results so obtained were compared. Here, we employ the CG method for the optimization of a cost functional within QOCT, formulated by Rabitz and coworkers [14,15] to control fundametal and overtone transitions using calculated *ab-initio* potential and dipole moment functions and the results of the effect of variation of the penalty factor on the physical attributes of the system and on the pulse shape for different time durations considered, are analysed. This is not done in the previous vibrational control of HCl molecule.

In this work, we carry out the calculation of optimal pulses and analysis of their spectral content and temporal profile within the framework of QOCT for vibrational control of the HCl molecule for the following transitions:

HCl($v = 0$) → HCl($v = 1$),

HCl($v = 0$) → HCl($v = 2$).
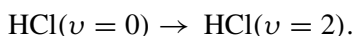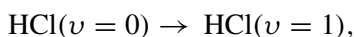
These calculations are done for three pulse durations, i.e., 30000, 60000 and 90000 a.u., for a given value of penalty factor. The suggested time-scales range from subpicosecond to picosecond time-scales in real time. Hence, the time-scales chosen are optimal guess to start with, for these vibrational transition calculations.

2. Quantum optimal control theory

2.1 *Formalism*

We formulate the problem such that we seek a desired value of an observable at $t = T$, by applying a field. In a realistic system, the field is not deterministic. There may be several sources of noise.

After the application of control field, $\epsilon(t)$, the Hamiltonian of the system can be written as follows:

$$\hat{H} = \hat{H}_0 + \hat{V} - \hat{\mu}[\epsilon(t) + \eta(t)], \tag{1}$$

where $\hat{\mu}$ is an electric dipole operator and $\eta(t)$ is a noise term.

This is within semiclassical dipole approximation [26,27].

The crucial step is to optimize a cost functional, $J[\epsilon(t)]$, given by (atomic units are used throughout the text, $\hbar = 1$)

$$J[\epsilon(t)] = |\langle \psi_i(T)|\phi_f\rangle|^2 - \alpha_0 \int_0^T \epsilon(t)^2 \mathrm{d}t$$

$$- 2\mathrm{Re}\left[\int_0^T \langle \chi_f(t)|\frac{\partial}{\partial t} + i\hat{H}|\psi_i(t)\rangle\right]. \tag{2}$$

The function $\psi_i(t)$ is the initial wave function propagated in time t by the optimal laser field, $\epsilon(t)$, and ϕ_f is the target state specified at the final time, T. The function $\chi_f(t)$ can be regarded as a Lagrange multiplier function introduced to assure satisfaction of the Schrödinger equation. The factor α_0 is a positive weighting parameter to adjust the contribution of the radiation energy to the functional.

The first term in eq. (2) refers to the transition probability. Second term is a penalty term for the electric field strength with the weight α_0. The last term ensures the physics of the dynamics, the time-dependent Schrödinger equation (TDSE), that should be followed exactly.

Each of these terms depends explicitly or implicitly on the unknown driving field, $\epsilon(t)$, and the goal is to maximize $J[\epsilon(t)]$ by demanding $(\partial J[\epsilon]/\partial\epsilon) = 0$. Setting the first-order variations of the cost functional with

respect to $\chi_f(t)$, $\psi_i(t)$, and $\epsilon(t)$ to zero yield, we get the following nonlinear pulse design equations:

$$\frac{\partial J}{\partial \chi_f} = 0 \Rightarrow i \frac{\partial \psi_i(t)}{\partial t} = \hat{H} \psi_i(t),$$
$$\psi_i(0) = \phi_i, \tag{3}$$

$$\frac{\partial J}{\partial \psi_i} = 0 \Rightarrow i \frac{\partial \chi_f(t)}{\partial t} = \hat{H} \chi_f(t),$$
$$\chi_f(T) = \langle \phi_f | \psi_i(T) \rangle | \phi_f \rangle, \tag{4}$$

$$\frac{\partial J}{\partial \epsilon} = 0 \Rightarrow \alpha_0 \epsilon(t) = -\mathrm{Im}(\langle \chi_f(t) | \mu | \psi_i(t) \rangle). \tag{5}$$

The desired field can be obtained from eq. (5). The numerical complexity of solving these equations arises because eq. (3) gives the evolution of the initial state in time. Equation (4) gives the magnitude of $\chi(t)$ at $t = T$, and both are required at each point of time to calculate the field. In general, these coupled differential equations should be solved iteratively due to their nonlinear nature.

3. Conjugate gradient method

The laser field, $\epsilon(t)$, is given by

$$\epsilon(t) = s(t) \cdot \epsilon_0(t), \tag{6}$$

where $s(t)$ is the Gaussian envelope which ensures smooth decay of the laser field $\epsilon(t)$ at initial and final time and $\epsilon_0(t)$ is a sinusoidal function. The envelope function, $s(t)$, implemented is given by

$$s(t) = \exp \frac{-(t - T/2)^2}{(T/4)^2}, \tag{7}$$

where T is the total time of pulse duration. The gradient of J with respect to $\epsilon_0(t)$ at time t after k number of iterations in the optimization cycle is written as

$$g^k(t) = \frac{\partial J^k}{\partial \epsilon_0^k(t)}$$
$$= -2s(t) \left[\alpha_0 \epsilon^k(t) - \mathrm{Im} \langle \chi(t) | \frac{\partial \hat{H}}{\partial \epsilon^k(t)} | \psi(t) \rangle \right]. \tag{8}$$

Both $\psi(t)$ and $\chi(t)$ are propagated in time using the split-operator technique [28,29]. The time evolution is done in discrete time steps (t_i). One can proceed to search for the parameter space of the electric fields $\epsilon(t_i)$ that maximizes the cost functional value. Then a line search is performed along the Polak–Ribiere–Polyak search direction [30]. The search direction is defined as follows:

$$d^k(t_i) = g^k(t_i) + \lambda^k \cdot d^{k-1}(t_i), \tag{9}$$

where the conjugate gradient parameter, λ^k, is given as

$$\lambda^k = \frac{\sum_i g^k(t_i)^T (g^k(t_i) - g^{k-1}(t_i))}{\sum_i g^{k-1}(t_i)^T g^{k-1}(t_i)}. \tag{10}$$

Here, T indicates the transpose, $k = 2,3,...,$ and $d^1(t_i) = g^1(t_i)$. During the line search, the search direction $d^k(t_i)$ is projected [31] to avoid higher values of $\epsilon(t_i)$ from the predefined range.

In order to achieve a pulse having simple frequency structure, the frequency range of the laser pulse has to be restricted within the specified range ($\omega_{\min} : \omega_{\max}$)
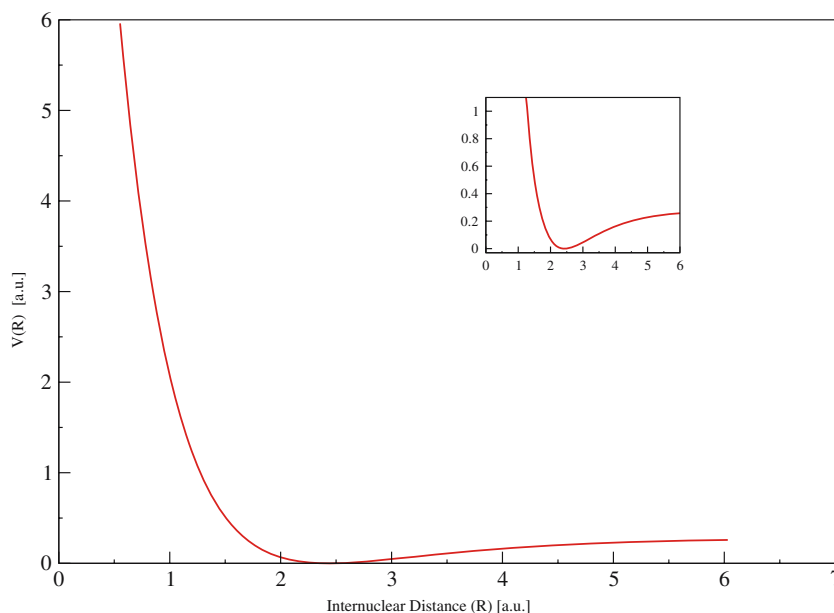
Figure 1. Potential energy curve for HCl: Morse potential calculated by *ab-initio* CCSD method with aug-cc-pVTZ basis set.
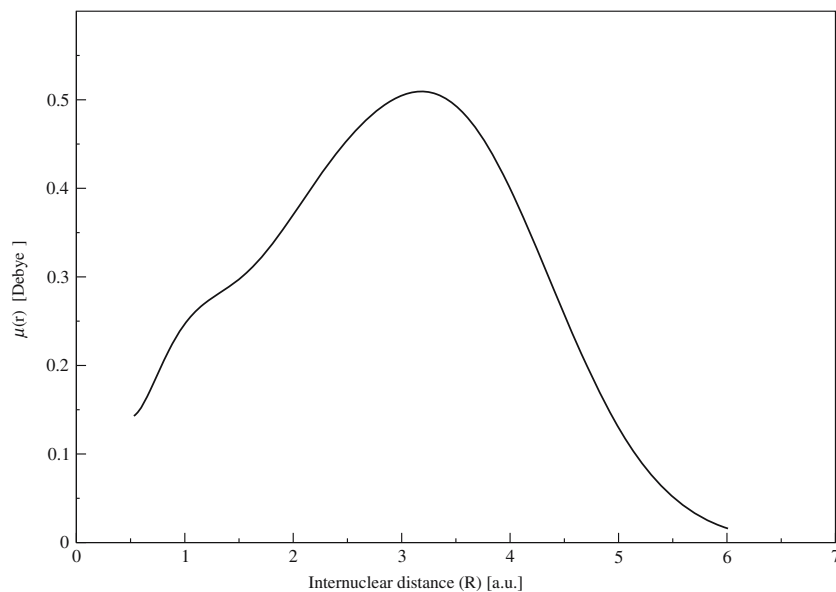
Figure 2. Dipole moment curve for HCl: calculated by *ab-initio* CASSCF(8,8) method with aug-cc-pVTZ basis set.
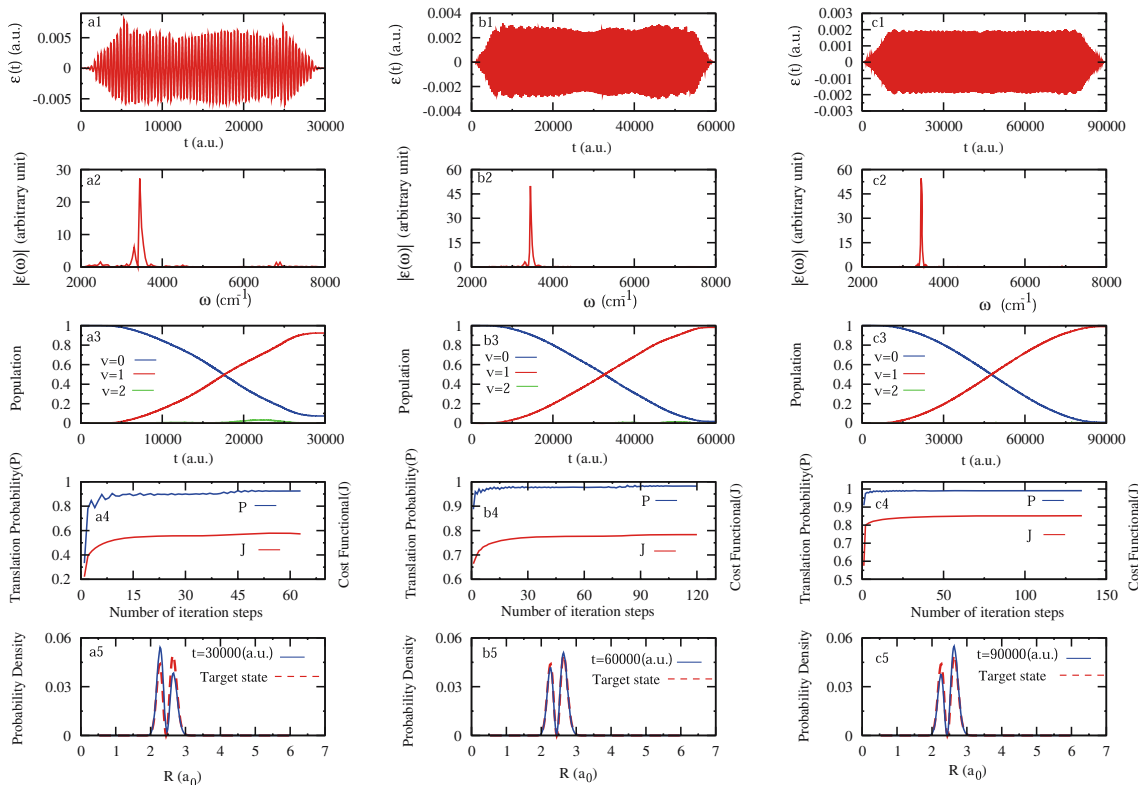
Figure 3. Optimized laser fields as a function of time (**a1**, **b1** and **c1**), frequency spectra of the optimized laser fields (**a2**, **b2** and **c2**), population dynamics of vibrational states (**a3**, **b3** and **c3**) and convergence of the transition probability, *P*, and the cost functional, *J*, with the number of iterative steps involved in the optimization (**a4**, **b4** and **c4**) are shown. Plots **a5**, **b5** and **c5** show the overlap of laser-driven evolved probability density at the end of pulse duration (shown as the blue curve) with the target probability density, for transition $\upsilon = 0 \rightarrow 1$ for pulses of duration 30000, 60000 and 90000 a.u.; α_0 is set as 1.0.

Table 1. Results for fundamental transition ($\upsilon = 0 \rightarrow \upsilon = 1$) for pulses of duration 30000, 60000 and 90000 a.u. for $\alpha_0 = 1.0, 0.1$ and 0.01. P refers to the transition probability, J refers to the cost functional value, ϵ_{peak} refers to the value of maximum amplitude of the optimized laser field. All quantities are in atomic units.

α_0	Pulse duration (T)	P	J	ϵ_{peak}
	30000	0.924	0.523	0.802×10^{-2}
1.00	60000	0.982	0.783	0.323×10^{-2}
	90000	0.990	0.852	0.203×10^{-2}
	30000	0.998	0.943	0.883×10^{-2}
0.10	60000	0.999	0.975	0.355×10^{-2}
	90000	0.999	0.983	0.241×10^{-2}
	30000	0.999	0.993	1.028×10^{-2}
0.01	60000	0.999	0.997	0.505×10^{-2}
	90000	0.999	0.999	0.344×10^{-2}

[32]. The frequency filtering is done with a 20th-order Butterworth band-pass filter [33] by filtering the projected search direction,

$$h(\omega) = \left[\left(1 + \left(\frac{\omega_{\text{min}}}{\omega} \right)^{40} \right) \left(1 + \left(\frac{\omega}{\omega_{\text{max}}} \right)^{40} \right) \right]^{-1/2}. \quad (11)$$

The projected search direction is Fourier transformed to obtain a function of frequency, and this function is further multiplied by $h(\omega)$ and transformed back to the time domain, which can be expressed as
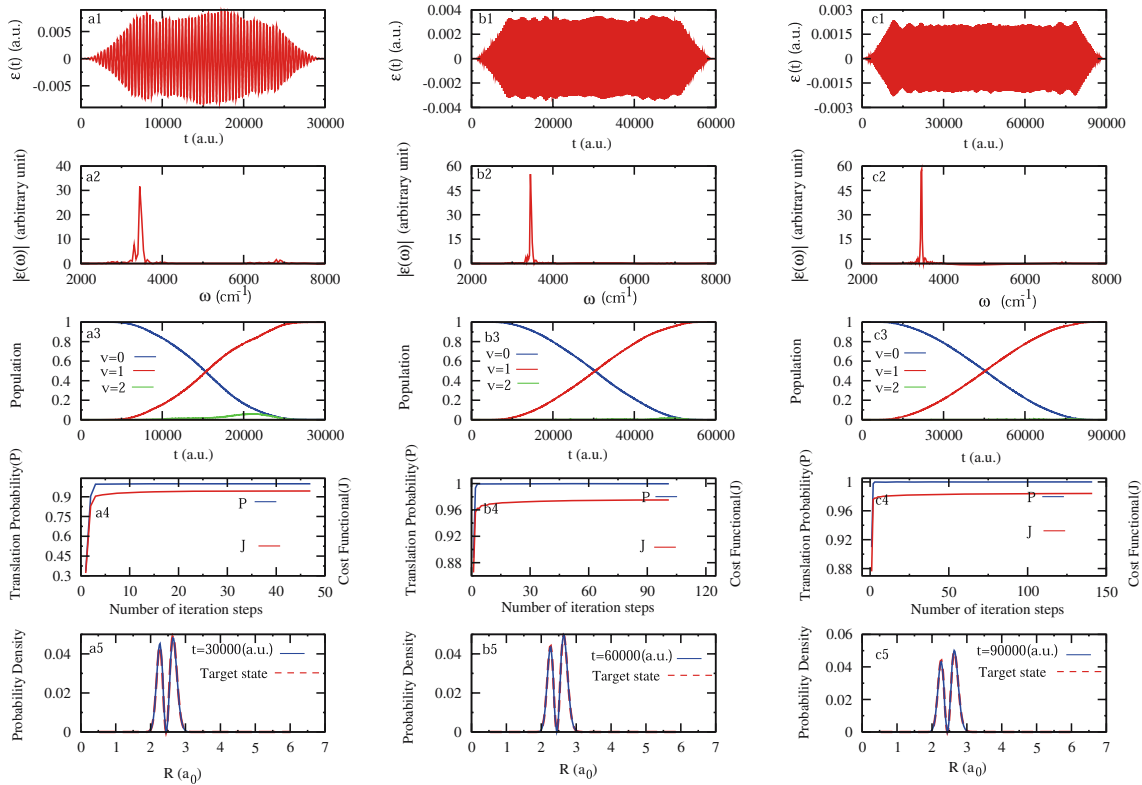
$$d_{p,\text{filter}}^k(t) = \int h(\omega) F_\omega[d_p^k(t)] e^{-i\omega t} d\omega, \quad (12)$$

where $F_\omega[d_p^k(t)]$ is the Fourier component at frequency ω.

The updated electric field is expressed as

$$\epsilon^{k+1}(t_i) = \epsilon^k(t_i) + \lambda s(t_i) d_{p,\text{filter}}^k(t_i), \quad (13)$$

where λ is determined by the line search.

Figure 4. Optimized laser fields as a function of time (**a1**, **b1** and **c1**), frequency spectra of the optimized laser fields (**a2**, **b2** and **c2**), population dynamics of vibrational states (**a3**, **b3** and **c3**) and convergence of the transition probability, P, and the cost functional, J, with the number of iterative steps involved in the optimization (**a4**, **b4** and **c4**) are shown. Plots **a5**, **b5** and **c5** show the overlap of laser-driven evolved probability density at the end of pulse duration (shown as the blue curve) with the target probability density, for transition $\upsilon = 0 \rightarrow 1$ for pulses of duration 30000, 60000 and 90000 a.u.; α_0 is set as 0.1.

4. Model system and *ab-initio* calculations

HCl molecule in its ground electronic state is considered as the model system. Potential and dipole moment functions are shown in figures 1 and 2, respectively. They are obtained by plotting the data calculated by *ab-initio* CCSD method with aug-cc-pVTZ basis and CASSCF(8,8) method with aug-cc-pVTZ basis set, respectively, using the Molpro suite of the program package [34]. The ground and excited state potentials are obtained by curve fitting as follows:

$$V(R) = D_e[1 - e^{-\beta(R-R_e)}]^2, \tag{14}$$

where $D_e = 0.278475$, $R_e = 2.412412037$ and $\beta = 0.918055$ in a.u., and the dipole moment operator is given as

$$\mu(R) = \sum_{n=0}^{6} \mu_n R^n e^{-\sigma R^2}, \tag{15}$$

where μ_0 to μ_6 values are: 1.06511, -5.2444, 10.9834, -10.7007, 5.51494, -1.43929, 0.159831, respectively, and $\sigma = 0.316883$ (in a.u.).

4.1 *One-dimensional treatment*

For a simple one-dimensional treatment, it is assumed that the HCl molecule is oriented along the direction of the linearly polarized laser field. The molecular Hamiltonian and the interaction Hamiltonian take the following forms:

$$\hat{H}_0 = \frac{-1}{2m}\frac{\partial^2}{\partial R^2} + V(R), \tag{16}$$

$$\hat{H}_{\text{int}} = -\mu(R)\cdot \epsilon(t), \tag{17}$$

where, $V(R)$ and $\mu(R)$ are of the form given in eqs (14) and (15), m is the reduced mass of HCl molecule and $\epsilon(t)$ is the electric field amplitude.

5. Results and discussion

In this section, results for the population control of the fundamental and overtone transition of the HCl molecule from its ground vibrational state to the desired target state are discussed within the dipole
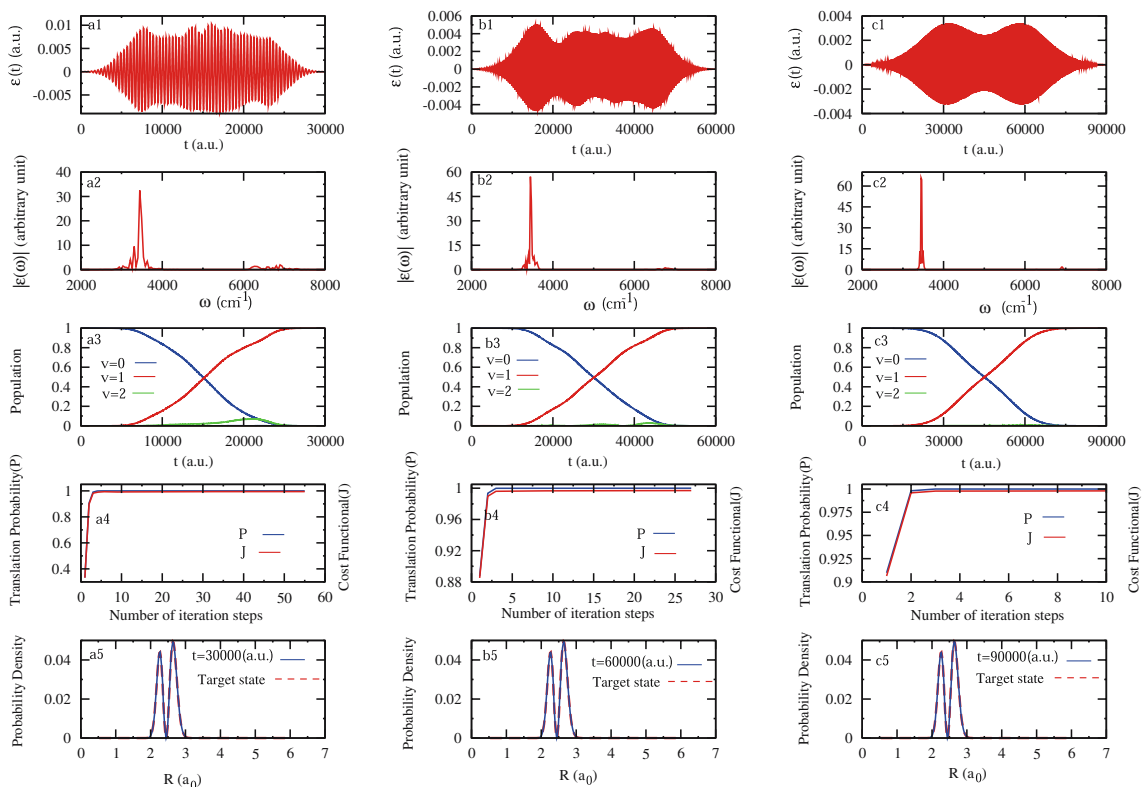
Figure 5. Optimized laser fields as a function of time (**a1**, **b1** and **c1**), frequency spectra of the optimized laser fields (**a2**, **b2** and **c2**), population dynamics of vibrational states (**a3**, **b3** and **c3**) and convergence of the transition probability, *P*, and the cost functional, *J*, with the number of iterative steps involved in the optimization (**a4**, **b4** and **c4**) are shown. Plots **a5**, **b5** and **c5** show the overlap of laser-driven evolved probability density at the end of pulse duration (shown as the blue curve) with the target probability density, for transition $\upsilon = 0 \rightarrow 1$ for pulses of duration 30000, 60000 and 90000 a.u.; α_0 is set as 0.01.

approximation. The Fourier grid Hamiltonian (FGH) [35–37] method is used to compute the vibrational energies and eigenfunctions of the model system. The nuclear wave function is represented on a one-dimensional grid along the internuclear coordinate, R; its magnitude ranging from $0.530a_0$ to $6.031a_0$.

The initial guess laser field has the following form:

$$\epsilon(t) = E_0 \sin(\omega_{\text{init}}t) \cdot s(t), \tag{18}$$

where E_0 is the field amplitude and $\omega_{\text{init}} = \omega_f - \omega_i$ corresponds to the frequency for transition from the initial to the target vibrational state of the HCl molecule. The factor, $s(t)$, is a Gaussian envelope function (eq. (7)) to ensure smooth decay of the pulse and is preserved during the optimization to design an experimentally feasible pulse. In eq. (11), ω_{min} and ω_{max} are set as 10 and 10000 cm^{-1}, respectively.

5.1 *Fundamental transition: HCl($\upsilon = 0$)→ HCl($\upsilon = 1$)*

Here, our goal is to design a suitable pulse at three different time durations, i.e., for $T = 30000, 60000$

and 90000 a.u., that can selectively transfer the population from the initial vibrational state to the target vibrational state. The initial guess amplitude, E_0, and the penalty factor, α_0, are set as 0.005 a.u. and 1.0, respectively.

In figure 3, plots a1, b1 and c1 show optimized electric fields as a function of time for pulse durations 30000, 60000 and 90000 a.u., respectively. It is clear from the structure of the pulses that as we increase the pulse duration the field amplitude decreases and the shape of the pulse gets broadened in the time domain, which is in accordance with the pulse-area theorem [38,39]. The associated frequency spectra for each pulse duration are shown in plots a2, b2 and c2. It is clear that the plot c2 shows sharp peak at 3447 cm^{-1} compared to plot a2 and plot b2 at their respective transition frequencies. The population transfer dynamics associated with the application of the pulse with durations 30000, 60000 and 90000 a.u., is shown in a3, b3 and c3 respectively. As time inceases, the population is transferred to the target state from the initial state for three pulse durations. During laser-driven dynamics,
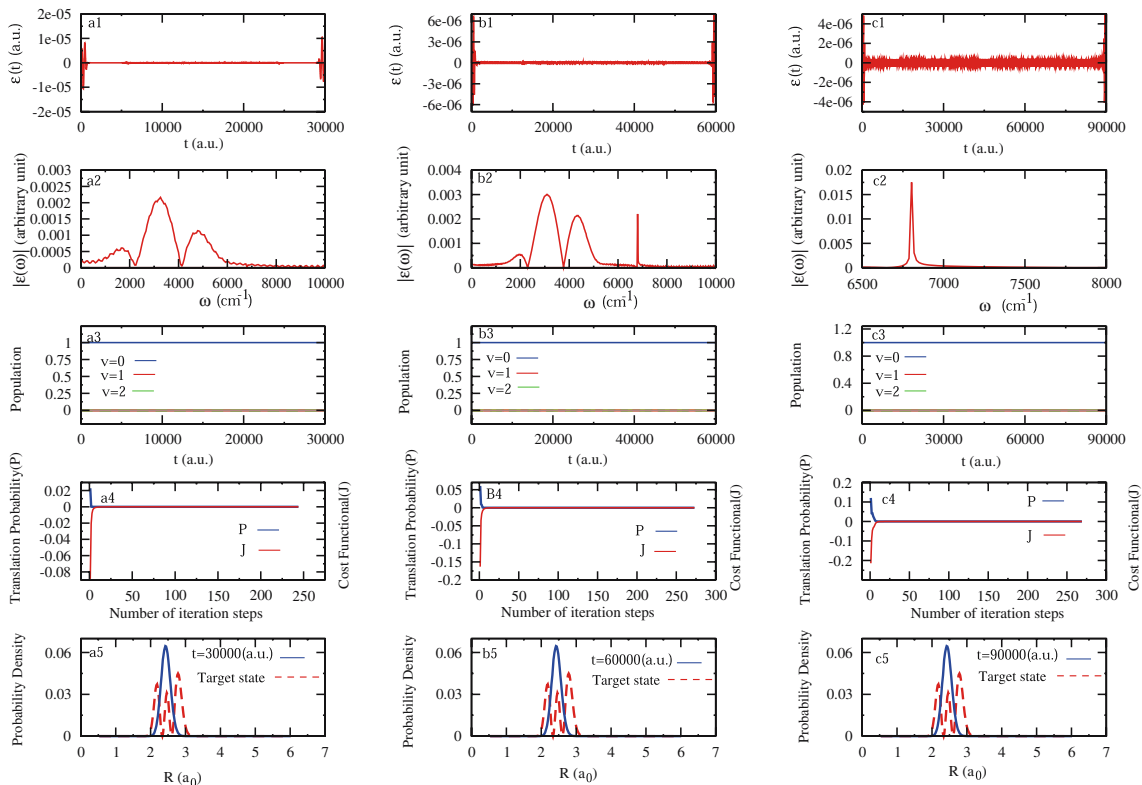
Figure 6. Optimized laser fields as a function of time (**a1**, **b1** and **c1**), frequency spectra of the optimized laser fields (**a2**, **b2** and **c2**), population dynamics of vibrational states (**a3**, **b3** and **c3**) and convergence of the transition probability, *P*, and the cost functional, *J*, with the number of iterative steps involved in the optimization (**a4**, **b4** and **c4**) are shown. Plots **a5**, **b5** and **c5** show the overlap of laser-driven evolved probability density at the end of pulse duration (shown as the blue curve) with the target probability density, for transition $\upsilon = 0 \rightarrow 2$ for pulses of duration 30000, 60000 and 90000 a.u.; α_0 is set as 1.0.

some of the population is transferred to the $\upsilon = 2$ state, considerably for the 30000 and 60000 a.u., pulses but negligibly small for the 90000 a.u. pulse. However, at the end of each pulse duration, 100% population transfer occurs to the target state (i.e., $\upsilon = 1$). The plots a4, b4 and c4 show the variation in transition probability and cost functional with iteration steps of optimization for each duration of pulse considered, respectively. The convergence of the algorithm is found to be faster for the 30000 a.u. pulse duration. After a few steps, for the application of 90000 a.u. pulse, the cost functional converges to a value 0.85 (plot c4) which corresponds to more than 99% population transfer.

The time evolution of the initial state probability densities under the action of the three pulses is shown in plots a5, b5 and c5 respectively at the end of their duration. They show good overlap for 30000 and 60000 a.u. pulse and complete overlap for 90000 a.u. pulse with target probability density at the final time, T, of each pulse.

We show in table 1 and in figures 4 and 5, the effect of penalty factor, α_0, on transition probability, P, cost

functional value, J and the field peak amplitude, ϵ_{peak}, by setting its value as 0.10 and 0.01 respectively for three pulse durations. It is observed that for $\alpha_0 = 0.01$, the three pulses of duration 30000, 60000 and 90000 a.u. are almost equally efficient in transferring population to the target state following an expected trend of decrease in field amplitudes and increase in probability densities and higher values of cost functional and its faster convergence with the increase of time duration. Exactly the same arguments would go through for $\alpha_0 = 0.1$ also, but with slightly less performance in driving population to the target state, comparatively.

5.2 *Overtone transition: HCl($\upsilon = 0$)$\rightarrow$ HCl($\upsilon = 2$)*

As for the fundamental transition, here too, we aim to design suitable pulse for three different time-scales of pulse duration that can achieve maximum population transfer selectively to the target state. We observed that for this transition, α_0 plays a crucial role for all the three time-scales in the design of optimal pulses. Here, in
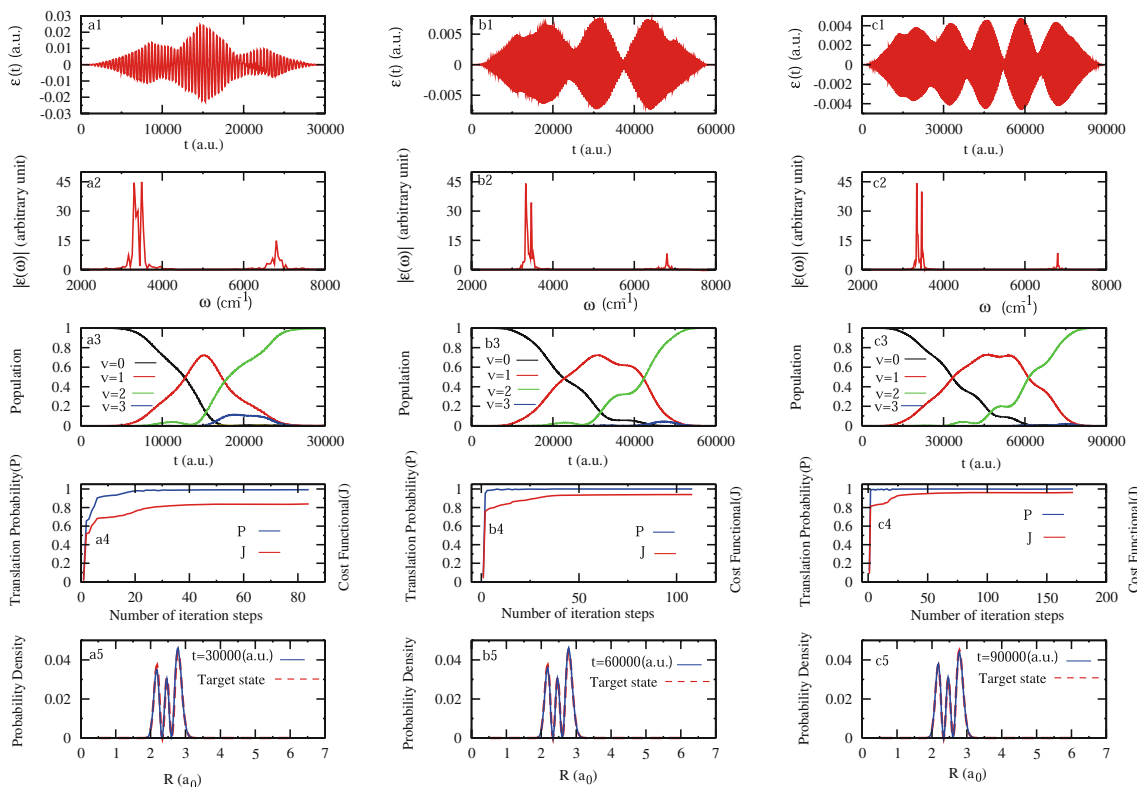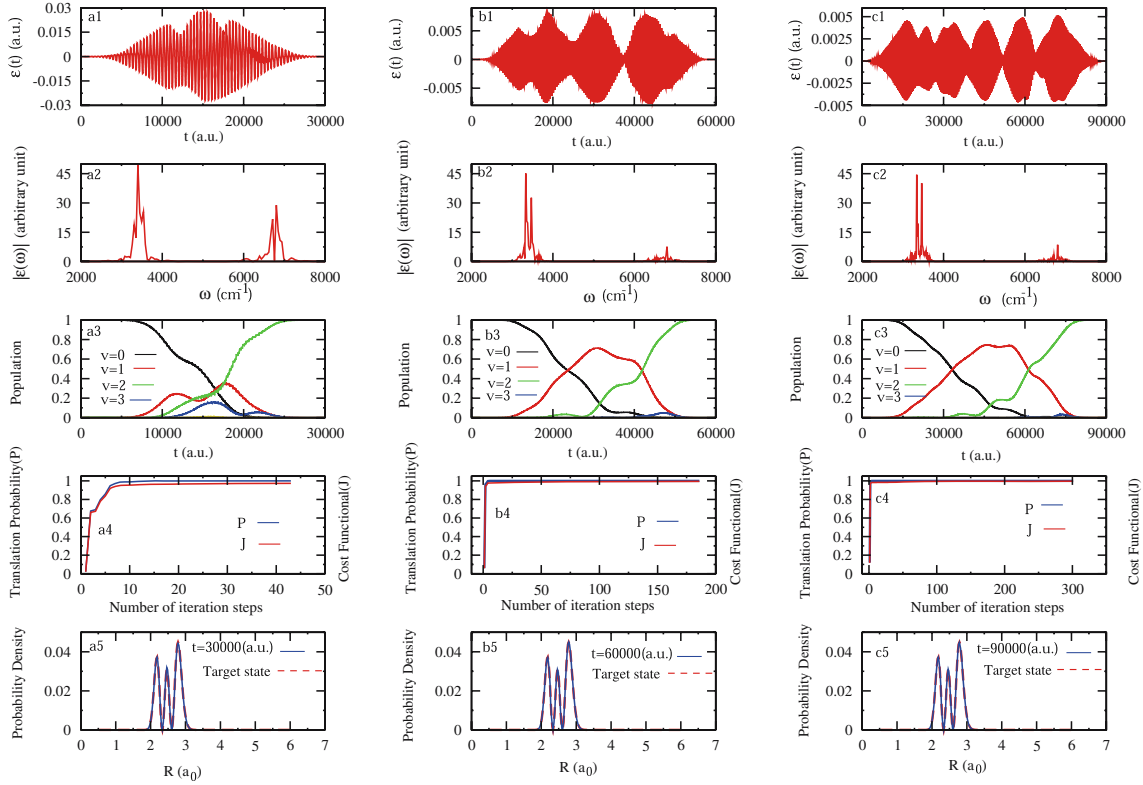

Figure 7. Optimized laser fields as a function of time (**a1**, **b1** and **c1**), frequency spectra of the optimized laser fields (**a2**, **b2** and **c2**), population dynamics of vibrational states (**a3**, **b3** and **c3**) and convergence of the transition probability, P, and the cost functional, J, with the number of iterative steps involved in the optimization (**a4**, **b4** and **c4**) are shown. Plots **a5**, **b5** and **c5** show the overlap of laser-driven evolved probability density at the end of pulse duration (shown as the blue curve) with the target probability density, for transition $\upsilon = 0 \rightarrow 2$ for pulses of duration 30000, 60000 and 90000 a.u.; α_0 is set as 0.1.

this case, for instance, setting α_0 to 1.0 with amplitude, $E_0 = 0.005$ a.u. leads to an optimized field with secondary frequency structure and showing highly poor performance in mimicking the initial state with the target state. The results for $\alpha_0 = 1.0$ are shown in figure 6.

As we decrease the penalty factor by a factor of 10 twice successively and run the optimization calculations,

Figure 8. Optimized laser fields as a function of time (**a1**, **b1** and **c1**), frequency spectra of the optimized laser fields (**a2**, **b2** and **c2**), population dynamics of vibrational states (**a3**, **b3** and **c3**) and convergence of the transition probability, *P*, and the cost functional, *J*, with the number of iterative steps involved in the optimization (**a4**, **b4** and **c4**) are shown. Plots **a5**, **b5** and **c5** show the overlap of laser-driven evolved probability density at the end of pulse duration (shown as the blue curve) with the target probability density, for transition $\upsilon = 0 \rightarrow 2$ for pulses of duration 30000, 60000 and 90000 a.u.; α_0 is set as 0.01.

Table 2. Results for overtone transition ($\upsilon = 0 \rightarrow \upsilon = 2$) for pulses of duration 30000, 60000 and 90000 a.u. for $\alpha_0 = 1.0$, 0.1 and 0.01. *P* refers to the transition probability, *J* refers to the cost functional value, ϵ_{peak} refers to the value of maximum amplitude of the optimized laser field. All quantities are in atomic units.

α_0	Pulse duration (T)	P	J	ϵ_{peak}
	30000	4.8680×10^{-12}	-9.4845×10^{-8}	0.10622×10^{-6}
1.00	60000	5.3980×10^{-10}	-1.1048×10^{-7}	6.8567×10^{-6}
	90000	1.04212×10^{-8}	-1.6954×10^{-7}	4.985×10^{-6}
	30000	0.9920	0.8385	2.43×10^{-2}
0.10	60000	0.9991	0.9393	0.78×10^{-2}
	90000	0.9996	0.9618	0.48×10^{-2}
	30000	0.9996	0.9730	2.76×10^{-2}
0.01	60000	0.9999	0.9935	0.83×10^{-2}
	90000	0.9999	0.9959	0.51×10^{-2}

we begin to see efficient population transfer to an intermediate state ($\upsilon = 1$) and a small amount to the higher state ($\upsilon = 3$) but with a fair amount of population transference to the target state ($\upsilon = 2$) involved during the laser-driven dynamics for all three time-scales. However, at the end of pulse durations, the entire population is transferred to the target state. The secondary structure of the frequency spectrum for each pulse duration is fairly reduced for $\alpha_0 = 0.01$ and 0.1. However, the reduction of the secondary structure of frequency is better for $\alpha_0 = 0.01$, compared to $\alpha_0 = 0.1$. The width in the peaks accounts for involvement of other states during population transfer dynamics. We can also observe that, as we decrease the α_0 value from 1.0, the pulse has complex temporal behaviour for all three pulse durations considered. The interesting fact observed for two α_0 values, with each involving three different time-scale pulses is that, as pulse duration increases, the splitting of initial Gaussian-enveloped pulse into a train of subpulses, shows that excitation with a train of pulses is needed to achieve maximum population transfer to the target for overtone transition unlike fundamental transition. It is clear that the pulse structure accounts for small oscillations of population of the initial and the target states, during the laser-driven dynamics. The effect of oscillation of population is more pronounced for 90000 a.u. pulse for both α_0 values, as is revealed by its pulse stucture compared to 30000 and 60000 a.u. However, it is much more pronounced for $\alpha_0 = 0.01$. The results are shown in plots of figures 7 and 8 for $\alpha_0 = 0.1$ and 0.01, respectively.

We show in table 2 and in figures 7 and 8, the effect of α_0 on the transition probability, P, the cost functional, J, the field peak amplitudes, ϵ_{peak}, by varying its value to 1.0, 0.10 and 0.01, for three different pulse durations for each value of α_0. Here too, it is observed that for $\alpha_0 = 0.01$, the three pulses of duration 30000, 60000 and 90000 a.u. are almost equally efficient in transferring population to the target state, following a trend in the amplitudes, the cost functional convergence and the probability densities, as expected, as is explained earlier in fundamental transition control.

6. Conclusions

Reliable optimized laser fields are obtained using the CG method within the framework of QOCT by considering the calculated *ab-initio* potential and dipole moment functions. As expected, we observed that for each pulse duration considered, with decrease in the value of the penalty factor α_0, the field amplitude increases. As we increase the pulse duration for a particular α_0, for the transitions treated in the text, the amplitude of field decreases. The results of the cost functional convergence with the variation of the penalty factor for the pulse durations considered, clearly illustrates the interplay of penalty factor and amplitude term in the penalty function, $(-\alpha_0 \int_0^T \epsilon(t)^2 \mathrm{d}t)$, with former always showing a dominating role. As we increase the time duration for a particular α_0, more iterative steps are needed for the convergence of transition probabilities. It is almost 100% transfer for both the transitions at the end of each pulse duration for $\alpha_0 = 0.1$ and 0.01. The optimized fields obtained with smooth switch on and off behaviour can possibly be implemented experimentally with judicious choice of other parameters such as α_0, T and ϵ_{peak} as discussed in the text for respective transitions considered here.

Acknowledgements

References

[1] K Moore and H Rabitz, *Nature Chem.* **4**, 72 (2012)

[2] A Assion, T Baumert, M Bergt, T Brixner, B Kiefer, V Seyfried, M Strehle and G Gerber, *Science* **282**, 919 (1998)

[3] R J Levis, G M Menkir and H Rabitz, *Science* **292**, 709 (2001)

[4] S Vajda, A Bartlet, E C Kaposta, T Leisner, C Lepulescu, S Minemoto, P Rosendo-Francisco and L Woste, *Chem. Phys.* **267**, 231 (2001)

[5] R J Gordon and S A Rice, *Annu. Rev. Phys. Chem.* **48**, 601 (1997)

[6] D J Tannor and S A Rice, *J. Chem. Phys.* **83**, 5013 (1985)

[7] D J Tannor, R Kosloff and S A Rice, *J. Chem. Phys.* **85**, 5805 (1986)

[8] P Brummer and M Shapiro, *Acc. Chem. Res.* **22**, 407 (1989)

[9] M Shapiro and P Brummer, *J. Chem. Phys.* **84**, 4103 (1986)

[10] P Brummer and M Shapiro, *Annu. Rev. Phys. Chem.* **43**, 257 (1992)

[11] T Baumert and G Gerber, *Isr. J. Chem.* **34**, 103 (1994)

[12] L C Zhu, V Kleiman, X N Li, S-P Lu, K Trentelman and R J Gordon, *Science* **270**, 77 (1995)

[13] David J Tannor, *Introduction to quantum mechanics* (University Science Books, Sausalito, California, 2007)

[14] S Shi and H Rabitz, *J. Chem. Phys.* **92**, 364 (1990)

[15] W Zhu, J Botina and H Rabitz, *J. Chem. Phys.* **108**, 1953 (1998)

[16] J Werschnik and E K U Gross, *J. Phys. B* **40**, R175 (2007)

[17] W Zhu, J Botina and H Rabitz, *J. Chem. Phys.* **108**, 1953 (1998)

[18] G G Balint-Kurti, S Zou and A Brown, *Adv. Chem. Phys.* **138**, 43 (2008)

[19] G G Balint-Kurti, F R Manby, Q Ren, M Artamonov, Tak-San Ho and H Rabitz, *J. Chem. Phys.* **122**, 084110 (2005)

[20] Q Ren, G G Balint-Kurti, F R Manby, M Artamonov, Tak-San Ho and H Rabitz, *J. Chem. Phys.* **124**, 014111 (2006)

[21] W H Press, S A Teukolsky, W T Vetterling and B P Flannery, *Numerical recipes in FORTRAN* (Cambridge University Press, London, 2000)

[22] T Brixner and G Gerber, *Chem. Phys. Chem.* **4**, 418 (2003)

[23] P Neuernberger, G Vogt, T Brixner and G Gerber, *Phys. Chem. Chem. Phys.* **9**, 2470 (2007)

[24] R S Judson and H Rabitz, *Phys. Rev. Lett.* **68**, 1500 (1992)

[25] S Sharma, H Singh and G G Balint-Kurti, *J. Chem. Phys.* **132**, 064108 (2010)

[26] K Sunderman and R de Vivie-Riedle, *J. Chem. Phys.* **110**, 1896 (1999)

[27] S P Shah and S A Rice, *J. Chem. Phys.* **113**, 6536 (2000)

[28] M D Feit and J A Fleck Jr, *J. Chem. Phys.* **78**, 301 (1983)

[29] M D Feit and J A Fleck Jr, *J. Chem. Phys.* **80**, 2578 (1984)

[30] E Polak, *Computational methods in optimization, mathematics in science and engineering* (Academic Press, New York, 1971) Vol. 77

[31] E G Birgin, J M Martinez and M Raydan, *SIAM J. Optim.* **10**, 1196 (2000)

[32] P Gross, D Neuhauser and H Rabitz, *J. Chem. Phys.* **96**, 2834 (1992)

[33] L R Rabiner and C M Rader (Eds), *Digital signal processing* (IEEE Press, New York, 1972)

[34] H-J Werner, P J Knowles, R D Amos, A Bernhardsson *et al MOLPRO-2002, a package of ab initio programs* (Universitat Stuttgart, Stuttgart, Germany; University of Birmingham, United Kingdom, 2002)

[35] C C Marston and G G Balint-Kurti, *J. Chem. Phys.* **91**, 3571 (1989)

[36] G G Balint-Kurti, C L Ward and C C Marston, *Comput. Phys. Commun.* **67**, 285 (1991)

[37] G G Balint-Kurti, R N Dixon and C C Marston, *Int. Rev. Phys. Chem.* **11**, 317 (1992)

[38] T Cheng and A Brown, *J. Chem. Phys.* **124**, 034111 (2006)

[39] M Holhaus and B Just, *Phys. Rev. A* **49**, 1950 (1994)